ICAS 2021 SHANG HAI
32nd Congress of the International Council of the Aeronautical Sciences
September 6-10, 2021
Pudong Shangri-La, Shanghai, China

Topology Optimization for Wing Structure of Hypersonic Vehicle

Shanshan Zhang1, Zhiqiang Wan1, Xiaozhe Wang2 & Yunzhen Liu3

[1]School of Aeronautic Science and Engineering, Beihang University, Beijing 100083, China
[2]Institute of Unmanned System, Beihang University
[3]China North Ind Grp Corp, Nav & Control Technol Inst

Abstract

Hypersonic vehicle has the characteristics of fast speed, long range, flexible mobility and rapid response, which can meet the needs of high-tech war and rapid transportation for military and civil use in the future. It has important strategic significance and high application value. Therefore, hypersonic vehicle technology is closely related to national security as a new frontier technology in the field of aerospace. Hypersonic vehicle represents the future direction of aerospace technology development, and is one of the focuses of aeronautics and astronautics research. An aerodynamic-thermo-structure coupling mechanism is proposed to achieve the integrated optimization of hypersonic wing surface in this paper. The results show that the structure is more favorable to heat load transfer after optimization. The results show that the proportion of thermal deformation in the total deformation decreases after the optimization design, which makes the structure form more favorable for heat load transfer.

Keywords: Hypersonic flight vehicle, Aero- thermo-structure coupling analysis, Topology optimization, Variable density method

1. Introduction

Hypersonic vehicles are defined as the aircrafts that are capable of flying through the atmosphere in a hypersonic speed five times faster than the sound.

The study of hypersonic vehicle began in 1949 when a WAC Corporal rocket transformed from a V-2 rocket captured by the United States was officially fired, which started the development of hypersonic vehicle[1]. Then, NASA developed the X-15 rocket-powered vehicle around the 1960s, which represented the direction of early hypersonic vehicle development[2][3].Subsequently, in the mid-1980s, the United States launched the National Aerospace Plane Program (NASP), which is the beginning of modern hypersonic vehicle research. In the research of hypersonic vehicle, how to meet the requirements of aerodynamic, thermal, structure, material, stealth, flight trajectory and other aspects of the aircraft through optimization and comprehensively improve the overall performance has always been the focus of research in various countries[4][5][6][7].

Generally speaking, Mach number 3-5 is taken as the boundary point between supersonic and hypersonic[8]. Hypersonic flow has many important inherent characteristics. The viscous coupling between the outer inviscid flow, the boundary layer and the shock wave in the airflow becomes very prominent[9]. The atmosphere dissociates and even becomes plasma, resulting in a chemical reaction boundary layer. This complex dynamic-thermal problem can only be analyzed by solving the complete unsteady Navier-Stokes (NS) equation while considering the real gas effect, which is a huge computational challenge[9].

Therefore, during hypersonic flight, aerodynamics, structure, thermology and other disciplines are coupled with each other and form a complex hypersonic aerothermoelastic problem[11]. As a difficult and key problem in this field, massive research has developed in many aspects, but a little is focused on the wing structure optimization of hypersonic vehicle.

In this paper, an advanced topology optimization framework for the wing structure of hypersonic flight vehicle using aero-thermo-structure coupling analysis is proposed. Based on the variable density method SIMP for continuum structure, a specific example model is analyzed to test this optimization framework.

2. Methodology

Aerodynamic heating, thermal conduction, aerodynamic force and structural deformation of the hypersonic vehicle are not simple unidirectional effects[12]. The accuracy of the one-way coupling analysis method is low because it rarely includes the feedback effects of structural deformation on airflow distribution and aerodynamic forces. The calculation process of the aero-thermo-structure three-field coupling analysis framework[13] for a hypersonic wing structure involves the separate solution of several disciplines and the interdisciplinary iterative solution, including aerodynamic force calculation at hypersonic speed, aerodynamic heat calculation, thermal conduction calculation, structural static/dynamic analysis, and the coupling analysis among them.

2.1 Aero-thermo-structure coupling analysis framework

Although the three-field coupling problem of hypersonic velocity is a complex multi-disciplinary coupling problem, the process is quite intuitive. From the perspective of action mechanism, this paper explains the process of hypersonic three-field coupling problem.

1) The airflow flows across the surface of the aircraft to generate aerodynamic force and aerodynamic heat;
2) Aerodynamic force deforms the structure, changes the surface of the aircraft, and in turn affects aerodynamic force;
3) On the other hand, through heat conduction, the aerodynamic heat flow gradually changes the temperature of the structure and affects the elastic modulus of the structure, thus influences the structural deformation. Meanwhile, the thermal strain caused by the uneven distribution of temperature generated by heat conduction also affects the structural deformation, and then affects the aerodynamic force. In addition, the new structure surface temperature distribution also affects the aerodynamic heat flow;
4) When the heat flow input of aerodynamic heat and the heat dissipation of the structure reach the balance (generally can be judged by the change of thermal load), the whole three-field coupling problem reaches the final balance.

The flowchart of the above hypersonic three-field coupling process is shown in Figure 1. The serial numbers in the figure correspond to the above four steps respectively.

In this paper, the coupling relationship between various disciplines is analyzed, some sub-problems are decoupled, and the coupling problem is solved by iterative method. The focus of this paper is the construction of the comprehensive optimization framework for the wing structure of hypersonic vehicle. Therefore, the following four aspects are set:

1) Choose a flexible loose-coupling method as calculation method;
2) Use the two-way coupling method, as the double rhomboid trapezoid wing commonly used in literature as the example is obviously affected by aerodynamic heat.
3) Only considers the strong coupling problem, as the weak coupling relation has little influence on the three-field coupling process
4) Only structural static aeroelastic analysis is considered in the aeroelastic analysis of the three-field coupling analysis framework.

Based on the three-field coupling analysis ideas above, the three-field coupling analysis process in Figure 1 is extended to obtain the analysis framework for aerodynamic-thermo-structure coupling problems of hypersonic vehicle in Figure 2.

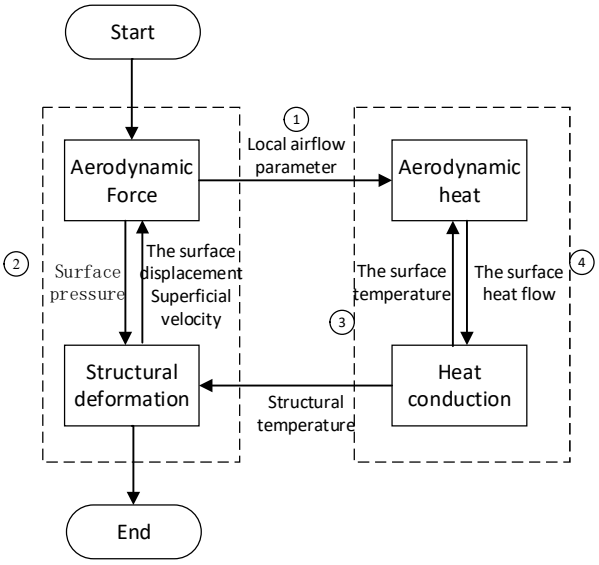

Figure 1 Hypersonic three-field coupling process

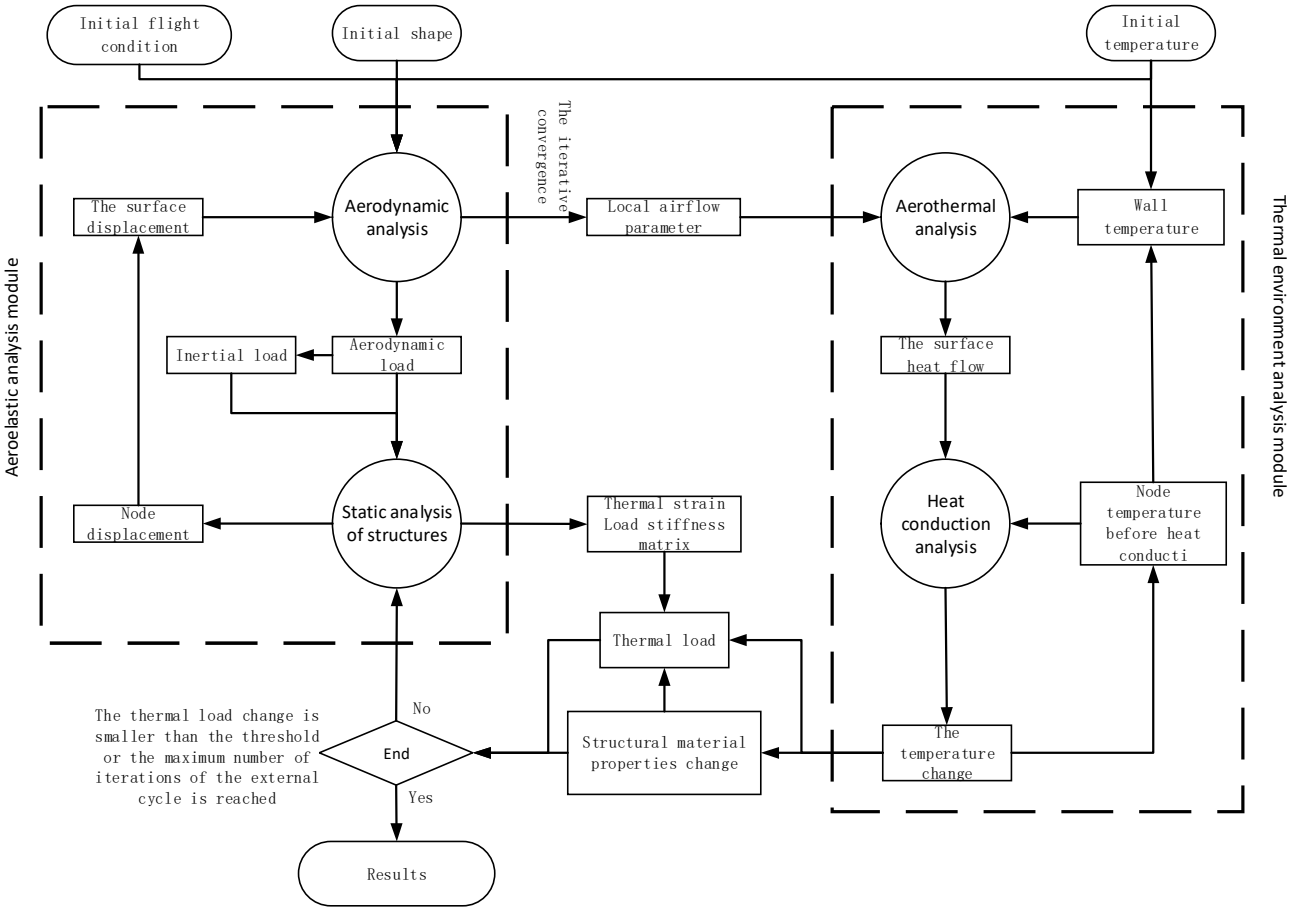

Figure 2 Aerodynamic-thermo-structure coupling analysis framework of hypersonic vehicle

The solution of aerodynamic-thermo-structure coupling problems of hypersonic vehicle can be divided into the following four main steps according to the above analysis framework:

1) Input the initial flight state, aerodynamic shape and temperature distribution to carry out the

iterative coupling analysis of the inner cycle of the aeroelastic module until the structural displacement converges;

2) Input the local airflow parameters obtained after aeroelastic convergence and the wall temperature of the structure at this moment into the thermal environment analysis module. Obtain the surface heat flux by aerodynamic thermal analysis and the new structure temperature distribution and temperature variation by heat conduction analysis.
3) Obtain the new material properties of the structure from the new temperature distribution of the structure, the thermal strain according to the temperature change, and the corresponding equivalent thermal load according to the load stiffness matrix obtained from the static analysis of the structure. Thus, an outer cycle calculation is completed.
4) If the thermal load at this time still changes greatly compared with the thermal load of the outer cycle of the previous generation, the thermal load will be input into the aeroelastic analysis module to conduct aeroelastic analysis together with the aerodynamic load and inertial load; if the thermal load change is smaller than the threshold or the maximum number of iterations of the external cycle is reached, the three-field coupling analysis will be finished and the analysis results will be output.

The analysis and solving of the four disciplines of aerodynamic force, aerodynamic heat, thermal conduction and structural static/dynamic analysis are mainly involved in the three field coupling analysis of hypersonic aircraft.

In order to improve the calculation speed and accuracy and the engineering practicality of the integrated optimization structure topology, the specific methods are as follows:

(1) Aerodynamic calculation: use the engineering method combining the shock/expansion wave theory and the local flow piston theory to provide the flow field parameters.

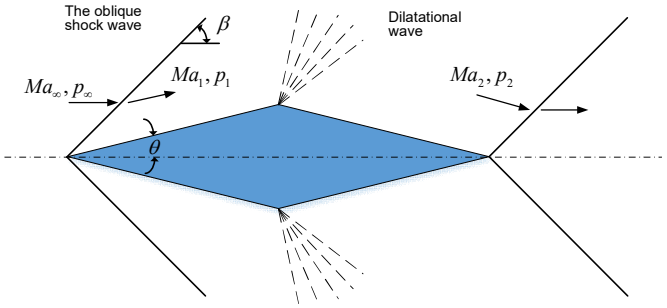

Figure 3 Shock/expansion wave theory

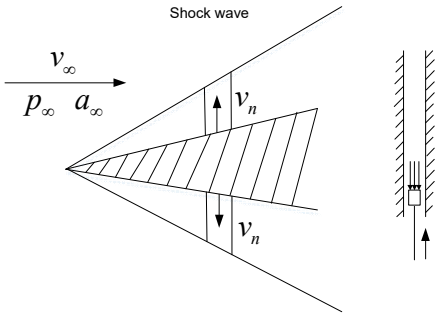

Figure 4 The local flow piston theory

The oblique shock wave formula[14] is

$$\tan\theta = 2\cot\beta \frac{Ma_\infty^2 \sin^2\beta - 1}{Ma_\infty^2(\gamma + \cos 2\beta) + 2} \tag{1}$$

The formula of local flow piston theory[15] is as follows:

$$C_p = \frac{2}{Ma_{local}^2}\left[\frac{v_n}{a_{local}} + \frac{(\gamma+1)}{4}\left(\frac{v_n}{a_{local}}\right)^2 + \frac{(\gamma+1)}{12}\left(\frac{v_n}{a_{local}}\right)^3\right] \tag{2}$$

The subscript local represents the local airflow parameter.

(2) Aerodynamic heat calculation: use Eckert reference temperature method[16] and blackbody radiation method[17].

The calculation formula of Eckert reference temperature method is as follows[18] :

$$T^* = 0.5T_w + 0.22T_r + 0.28T_e \tag{3}$$

Where T_w is the wall temperature; T_e is the temperature at the outer edge of the boundary layer, namely the local temperature of the flow field; T_r is the recovery temperature.

For compressible flows, the compressible modified Reynolds analogy is:

$$St^* = \frac{C_f^*}{2\,\mathrm{Pr}^{2/3}} \tag{4}$$

Heat flux calculation formula can be used in plate heat flux formula:

$$Q_{aero} = \rho_e u_e c_p \left(T_r - T_w\right) St^* \tag{5}$$

Since the surface of the panel at hypersonic speed is non-black body, the radiation heat dissipation formula is:

$$Q_{rad} = \sigma\varepsilon(T_w^4 - T_\infty^4) \tag{6}$$

Where σ is Stanford constant: 5.669E-8W /m2/T4, ε is the emissivity of non-blackbody surface radiation.

(3) Heat conduction calculation: use the Crank-Nicolson difference format based on the finite element method[19] to solve the analysis of transient thermal conduction problem[20].

The global finite element equation of the transient temperature field of the structure can be established by Galykin weighted residual method and element shape function as follows:

$$\boldsymbol{C}\dot{\boldsymbol{T}} + \boldsymbol{K}\boldsymbol{T} = \boldsymbol{P} \tag{7}$$

Where $\boldsymbol{C}$ is the overall heat capacity matrix, $\boldsymbol{K}$ is the overall temperature stiffness matrix, and $\boldsymbol{P}$ is the overall load column vector.

Crank-Nicolson difference format is:

$$\frac{\partial T(t)}{\partial t} + \frac{\partial T(t-\Delta t)}{\partial t} \approx 2\frac{T(t) - T(t-\Delta t)}{\Delta t} \tag{8}$$

Substitute it into Equation (7), then

$$\left(\boldsymbol{K} + \frac{2\boldsymbol{C}}{\Delta t}\right)\{T(t)\} = \{P(t)\} + \{P(t-\Delta t)\} + \left(\frac{2\boldsymbol{C}}{\Delta t} - \boldsymbol{K}\right)\{T(t-\Delta t)\} \tag{9}$$

(4) Structural static/dynamic calculation: use the finite element method.

(5) Thermal load analysis: use the thermal load equivalent method.

The force model for examining an element is

$$\int_{\Omega_e} \boldsymbol{B}^{\mathrm{T}} \boldsymbol{D}\left(\boldsymbol{\varepsilon} - \boldsymbol{\varepsilon}^T\right) = \int_{\Omega_e} \boldsymbol{B}^{\mathrm{T}} \boldsymbol{D}\left(\boldsymbol{B}\boldsymbol{u} - \boldsymbol{\varepsilon}^T\right) = \boldsymbol{F}_e \tag{10}$$

Where, $\mathbf{B}$ is the strain matrix, and $\mathbf{D}$ is the stress-strain relation matrix in the constitutive equation $\boldsymbol{\sigma} = \mathbf{D}\boldsymbol{\varepsilon}$

$$\boldsymbol{\varepsilon}^T = \left[\varepsilon_{xx}^T \quad \varepsilon_{yy}^T \quad \varepsilon_{zz}^T \quad \gamma_{xy}^T \quad \gamma_{xz}^T \quad \gamma_{yz}^T\right]^{\mathrm{T}} \tag{11}$$

Then for the global finite element equation,

$$\boldsymbol{K}\boldsymbol{U} = \boldsymbol{F} + \sum_e \int_{\Omega_e} \boldsymbol{B}^T \boldsymbol{D}\boldsymbol{\varepsilon}^T \tag{12}$$

Therefore, the thermal strain generated by the temperature gradient is equivalent to adding a

thermal stress load term to the right end of the original static balance equation of the structure, which is called the thermal load $\mathbf{F}_T$

$$\boldsymbol{F}_T = \sum_e \int_{\Omega_e} \boldsymbol{B}^T \boldsymbol{D} \boldsymbol{\varepsilon}^T \tag{13}$$

2.2 Structural topology optimization with variable density method

SIMP (Solid Isotropic Microstructures with Penalization) material interpolation model[21][22] is adopted in the topology optimization method of variable density method, with the formula as follows

$$E = \rho^p E_0 \tag{14}$$

The minimum compliance under the constraint of volume ratio (structure weight) is taken as the precondition for solving the structural topology optimization. The mathematical model is expressed as

$$\begin{aligned} &Find: \rho = \{\rho_1, \rho_2, ..., \rho_e\}^T \in R^n, e = 1, 2, ..., N \\ &\underset{x\in\Omega}{Min}: C(\rho) = F^T U = U^T K U = \sum_{e=1}^{N} u_e{}^T k_e u_e = \sum_{e=1}^{N} (\rho_e)^p u_e{}^T k_0 u_e \\ &s.t. \begin{cases} V(\rho)/V_0 - f \le 0 \\ KU = F \\ 0 < \rho_{\min} \le \rho_i \le \rho_{\max} \le 1 \end{cases} \end{aligned} \tag{15}$$

In the formula, C is the value of structural compliance; $\boldsymbol{K}$, $\boldsymbol{U}$ and $\boldsymbol{F}$ represent the total stiffness matrix, total displacement and total load of the structure respectively. V_0 represents the initial structure volume, V represents the structure volume of the optimization result, and f represents the ratio of the volume ratio to the previous two. $\rho_{\max}$ and $\rho_{\min}$ limit the variation range of topological variables, which is mainly used to avoid the singularity of finite element analysis. Usually, the lower limit of topological variables can be set as $\rho_{\min} = 10^{-3}$.

2.3 Comprehensive optimization framework

Based on the finite element method, the construction of the comprehensive optimization framework of the wing structure of hypersonic vehicle is achieved by nesting one layer topology optimization module outside the three-field coupling analysis framework shown in Figure 2.

The specific calculation process is described as follows:

(1) Define the initial conditions associated with the sublogy
The flight conditions and the initial wall temperature are defined in the program.

(2) Update the finite element model for the three-field coupling analysis according to the density threshold
The optimization area and the non-optimal area are divided based on the existing finite element model. As the design variable, the density properties are set separately for each element in the optimized area. The finite element model of the new wing surface topology is adjusted by the predetermined density threshold as the calculation model input for the three coupling analysis.

(3) Aerodynamic-thermo-structure coupling analysis
In view of the aerodynamic-thermo-structure coupling analysis framework of Figure 2, perform the aerodynamic-thermo-structure coupling analysis and convergence judgment: if the iteration step is reached, terminate the loop and output the result. If not, update aerodynamic shape, temperature field distribution and structure property, continue to loop.

(4) Perform the structure topology optimization based on the variable density method

Use the variable density method for topology optimization design based on the SIMP model[23][24]. Define the problem of topology optimization: define the objective function and constraints. The optimization variable is element density. The optimization process is as follows:

1) The temperature distribution, the stiffness matrix K_T of the heated structure and the thermal deformation U_T after the three-field coupling analysis are read from the program. The thermal load of the equivalent thermal load is calculated by the formula $\boldsymbol{F}_T = \boldsymbol{K}_T \boldsymbol{U}_T$, and is superposed with the aerodynamic force to obtain the total load and update the load condition.
2) The total load is taken as the boundary condition for the compliance calculation. After the first step of topology optimization, the program stops and the element density distribution in the optimization results is output.
3) Compare the two optimization results. When the volume ratio difference of the structure is less than the given convergence condition (the value of ε) or the maximum number of optimization steps is reached, the optimization ends. Otherwise, read the density optimization result, update the structural element density;
4) Screen the element density according to the density threshold. The elements with density value greater than or equal to the threshold value are left, and the rest elements are deleted. The finite element calculation model of the wing structure is updated, and the three-field coupling analysis is carried out again to enter the next generation topology optimization cycle calculation.

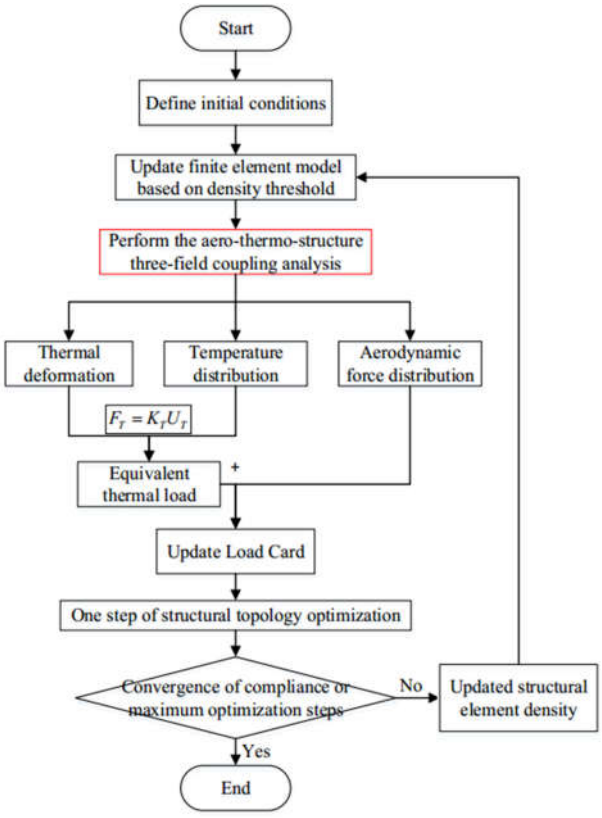

Figure 5 Flowchart of Integrated Optimization of Hypersonic Wing Structure

3. Modeling and strategy

3.1 Aanalytical model

The hypersonic wing structure model used in this paper is a typical wing structure of hypersonic

vehicle with a small ratio and rhombic airfoil. The main geometric parameters of the model are shown in Figure 6: the chord length of the wing root is $c = 5200mm$, the sweepvangle of the leading edge is 34°, the sweep angle of the trailing edge is 18°, and the maximum thickness of the wing structure is $d = (0.04c + 15.2)mm$, where $15.2mm = 4 \times 3.8mm$, $3.8mm$ corresponds to the single-layer thickness of the thermal protective layer on the upper and lower wing surfaces.
The finite element solid model and constraint conditions are shown in Figure 7.

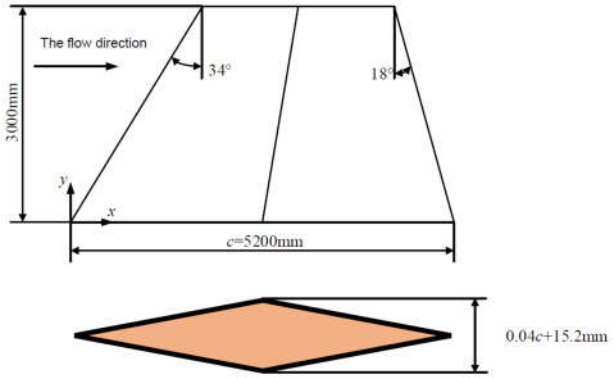

Figure 6 Schematic illustration of geometry parameters of hypersonic wing structure

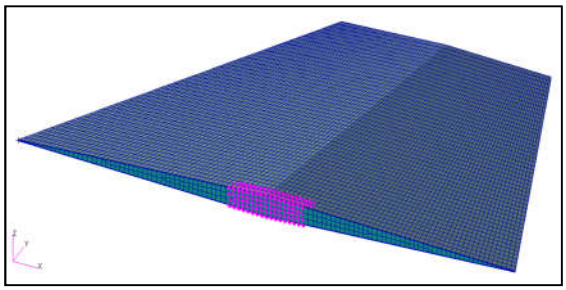

Figure 7 Solid finite element model of wing structure of hypersonic vehicle

3.2 Aerodynamic-thermo-structure coupling analysis parameters

The parameters of hypersonic Aerodynamic-thermo-structure coupling analysis are set as follows:

1) The Mach number is 8, the altitude is 15km，the angle of attack is 6°;
2) The initial temperature of the structure is 300K. In heat conduction analysis, the air specific heat ratio is 1.4, Plant number is 0.86, and the radiation emissivity is 0.85;
3) The time interval is 4s and the total computation time is 100s for the time scale of the aerodynamic heat flow and transient heat conduction.

3.3 Comprehensive optimization parameter

Based on the finite element model, the structure layer is divided into the optimization area (blue area in the center) and the non-optimization area (green area around), as shown in the figure below, after removing the non-optimization area of thermal protection layer and thermal insulation layer.

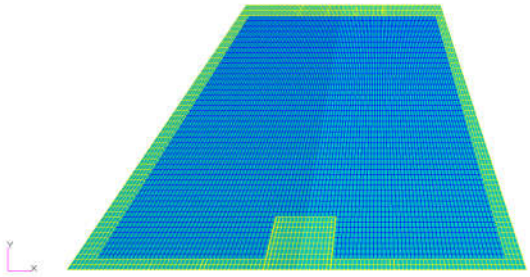

Figure 8 Schematic illustration of finite element optimization area (blue) and non-optimization area (green)

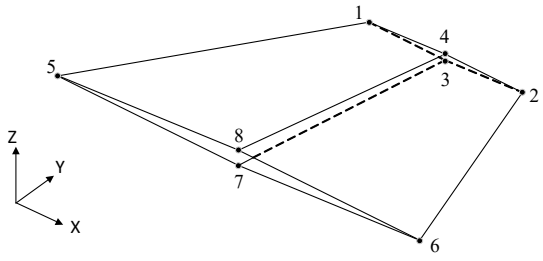

Figure 9 Schematic diagram of temperature monitoring points of structure

The objective function of topology optimization of the wing structure is defined as the minimization of structure compliance. The design variable is element density. Constraint conditions are that the structure volume ratio is less than 60%, and the displacements of the front and rear edge points of the wing root and tip and midpoint of the wing tip are less than 150mm. The element density

screening threshold of the updated finite element model is 0.5.
The parameters of the topology optimization are set as follows:
The Maximum Design Cycles (DSEMAX) limit is set as 50.
The Lower Bounds (XLB) of element density is set as XLB=0.001.
The Penalty Factor (1.0<POWER<=6.0) is set as POWER=3.
The maximum value of the design variable for each generation (Move Limit，0.01<=DELXV<=0.5) is set as 0.2.
The Minimum Member Size (TDMIN>0.1) is set as TDMIN= 200.
Set the number of topology optimization steps to 1.

4. Design results

4.1 The Aerodynamic-thermo-structure coupling analysis results of the original model

The Aerodynamic-thermo-structure coupling analysis is performed on the original model for comparative analysis with the subsequent optimized model.
In order to demonstrate the changing process of wing surface temperature during flight, the temperatures at 8 different structure positions as shown in Figure 9 are monitored. Points No.1 to No.4 correspond to the leading edge, trailing edge, lower vertex and upper vertex of the tip of the wing surface; points No.5 to No.8 correspond to the leading edge, trailing edge, lower vertex and upper vertex of the wing surface root.

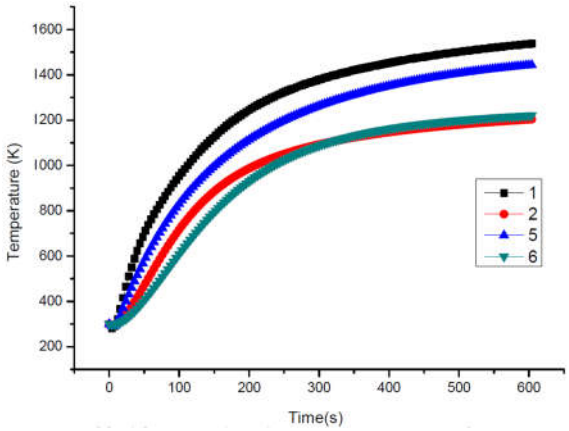

Figure 10 Temperature change process at points 1, 2, 5 and 6 of the wing structure

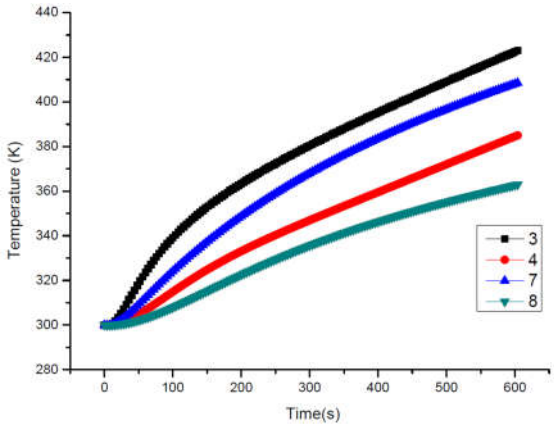

Figure 11 Temperature change process at points 3, 4, 7 and 8 of the wing structure

As shown in Figure 10 and Figure 11, during the flight time of 600s, the temperatures at the front and rear edges of the wing tip and wing root are relatively high, exceeding 1000K, and gradually tend to a certain stable value. The temperatures at the lower vertex and the upper vertex are better than that at the front and rear edges, and the temperatures rise slowly. Until 600s, the temperatures are still at 420K in the stage of slow rise.
Figure 12 to Figure 15 respectively show the pressure and heat flow distribution on the upper and lower surface of the airfoil at 0s and 600s.
At the time of 600s, the pressure is unevenly distributed on the whole wing surface due to the influence of the deformation of the wing structure. With the positive angle of attack, the aerodynamic pressure on the lower wing surface is higher than that on the upper wing surface, and the maximal pressure appears near the leading edge tip.
By comparing the heat flow distribution at 0s and 600s in Figure 14 and Figure 15, the heat flow on the wing surface in the initial flight state is far greater than that after 600s flight. This is because as the hypersonic flight time increases, the surface temperature keeps rising and the aerodynamic

heating and radiative heat dissipation of the aerodynamic surface gradually reach a balanced state.

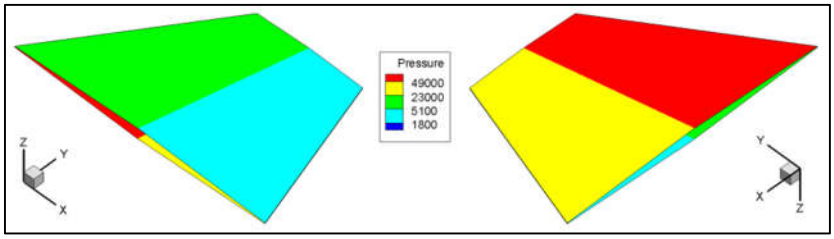

Figure 12 Pressure distribution on the airfoil surface (left) and lower surface (right) at 0s

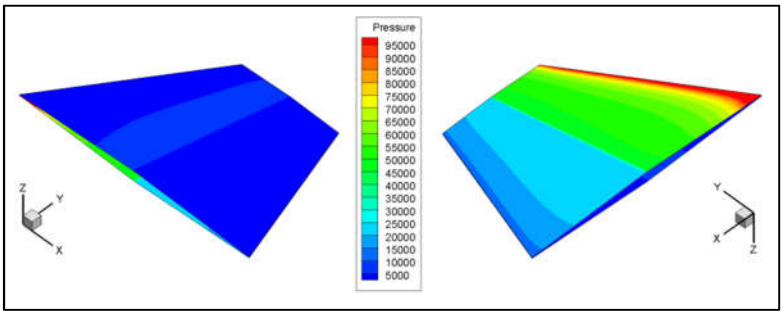

Figure 13 Pressure distribution on the airfoil surface (left) and lower surface (right) at 600s

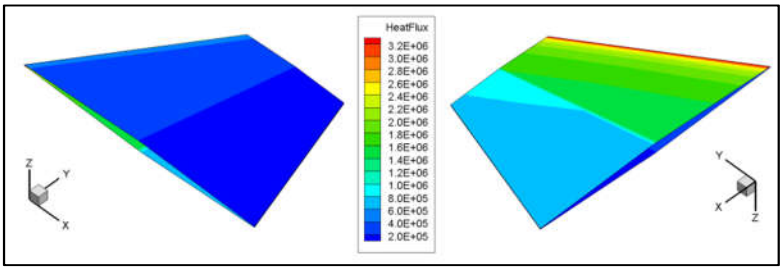

Figure 14 Heat flow distribution on the surface (left) and lower surface (right) of the airfoil at 0s

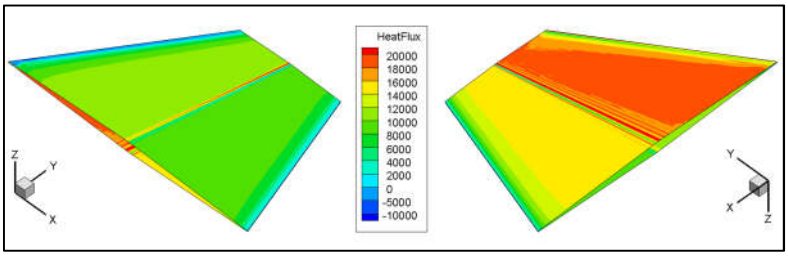

Figure 15 Heat flow distribution on the surface (left) and lower surface (right) of the airfoil at 600s

4.2 Topology optimization process of wing structure

Under the above optimization conditions, the hypersonic wing structure finally tends to converge after 17 generations of iterative calculation of topology optimization, and the convergence process of the structural compliance and optimized area volume ratio is shown in Figure 16 to Figure 17.

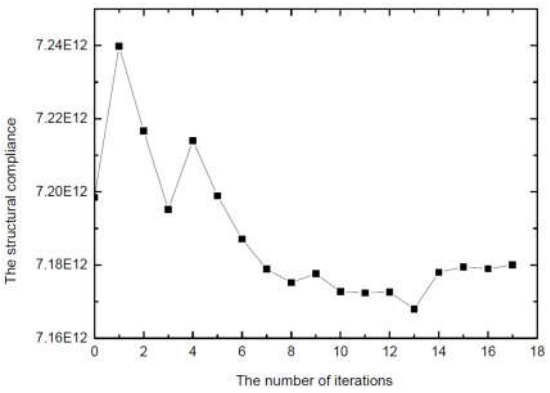

Figure 16 The structural compliance

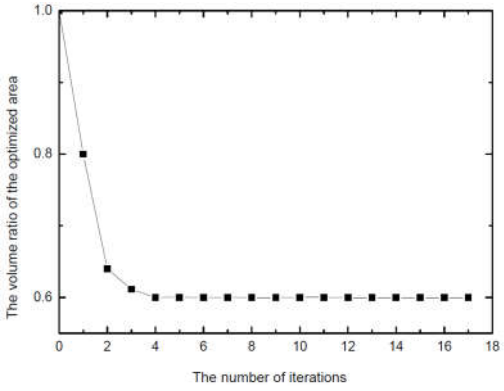

Figure 17 The the volume ratio of the optimized area

Table 1 The deformation, compliance and volume ratio of the wing structure in the optimization process

Iteration number	$u_{\max,F}$ /mm	$u_{\max,T}$ /mm	$u_{\max}$ /mm	C （J）	The volume ratio
0(Initial value)	15.4	102	113	7.1985E+12	100.0%
1	15.6	101	113	7.2398E+12	80.0%
2	18.7	96	110	7.2167E+12	64.0%
3	19.0	99	113	7.1952E+12	61.2%
4	18.9	100	114	7.2140E+12	60.0%
5	19.0	101	115	7.1989E+12	60.0%
6	18.9	104	117	7.1871E+12	60.0%
7	19.0	107	122	7.1789E+12	60.0%
8	19.0	111	126	7.1752E+12	60.0%
9	19.0	112	127	7.1776E+12	60.0%
10	18.9	111	125	7.1727E+12	60.0%
11	18.8	109	123	7.1724E+12	60.0%
12	18.8	107	122	7.1726E+12	60.0%
13	18.7	110	125	7.1680E+12	60.0%
14	18.7	112	127	7.1780E+12	60.0%
15	18.8	113	128	7.1795E+12	60.0%
16	18.8	115	129	7.1790E+12	60.0%
17	18.9	113	128	7.1800E+12	60.0%

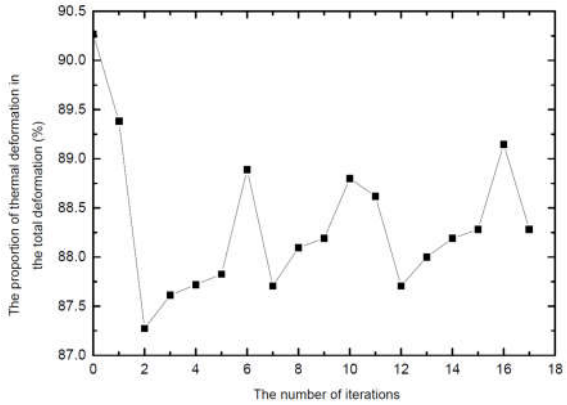

Figure 18 The proportion of thermal deformation in the total deformation

As can be seen from the results in the figures above, the structure compliance decreases and gradually converges to 7.18E+12. The volume ratio of the optimized region decreases rapidly from 100% to 60%, reaching near the boundary condition. In the iterative optimization process, the maximum displacement $u_{\max,F}$ under the action of aerodynamic force, the maximum displacement $u_{\max,T}$ under the action of thermal load, the maximum displacement $u_{\max}$ under the action of resultant force and the compliance C of the structure are shown in the following table. It should be noted that all displacements in the table are the statistical results at time of 100s.

As can be seen from the data in Table 1, with the process of structural topology optimization, the change of structural element density makes the structure develop in a direction more conducive to thermal load transmitting. Although the volume ratio decreases greatly (from 100% to 60%), the maximum thermal deformation changes mildly and the maximum displacement under aerodynamic load only increases slightly, indicating that the topology optimization can partly reduce the accumulation of thermal load. In addition, although both thermal deformation and aerodynamic deformation increases after 17 iterations, the proportion of thermal deformation in the total deformation decreases, as shown Figure 18.

After 17 generations of topology optimization, the topology form of the structure is gradually optimized from the solid configuration of the initial (n=0) to the perforated structure with obvious topology form in the 17th generation (n=17).

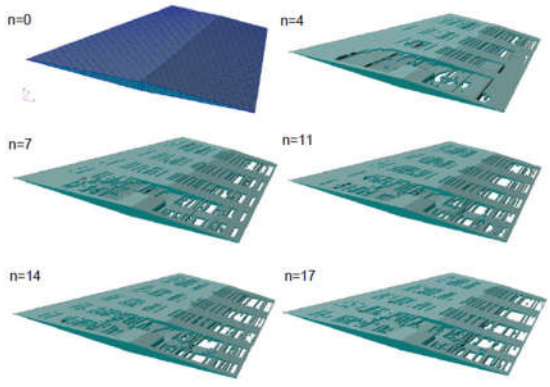

Figure 19 Topology optimization process of airfoil structure

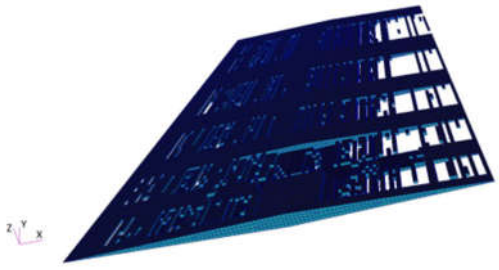

Figure 20 Schematic diagram of remaining elements in the optimized area after screening

After screening according to the density threshold of 0.5, the schematic diagram of the remaining structure can be obtained as shown in Figure 20. Based on the remaining structure after screening, the element density distribution in the optimal area of hypersonic wing structure is presented in

Figure 21 and Figure 22.

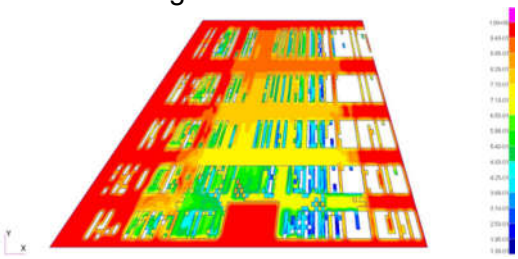

Figure 21 The density distribution on the upper surface of the region after optimization

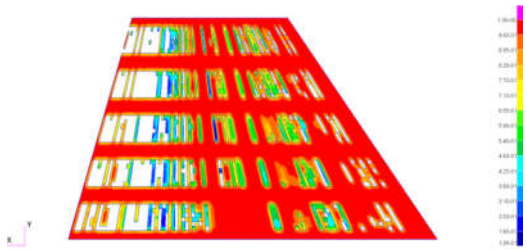

Figure 22 The density distribution on the lower surface of the region after optimization

It can be seen that there are four obvious transverse structures and most elements are retained on the lower wing surface of the inner wing segment. The result is related to the distribution of aerodynamic and thermal loads on the wing structure. The temperature of the lower surface is higher, the aerodynamic force and thermal load are greater than that of the upper surface, so more structures are needed to support the lower wing surface. The maximum displacement under thermal load occurs at the leading edge of the wing root, so more high-density elements are needed to strengthen the structure.

The temperature, pressure and heat flow distribution obtained from the three-field coupling analysis of the optimized wing structure are shown in the figure below. According to the optimized structure temperature distribution at 100s in Figure 24, it can be seen that at this time, the wing structure layer has not been fully heated and the structure temperature is generally lower than 350K, which is consistent with the temperature variation rule of upper and lower vertices inside the original model structure in Figure 11.

As can be seen from the optimized heat flow distribution on the wing surface at 100s in Figure 26, the heat flow at this time is of the order of 10^4, which is small compared with the initial heat flow size of 10^6 in Figure 14, indicating that the temperature of the aerodynamic surface is slowly approaching stability, which is consistent with the temperature variation rule of the original model near the front and rear edge monitoring points on the wing surface in Figure 10.

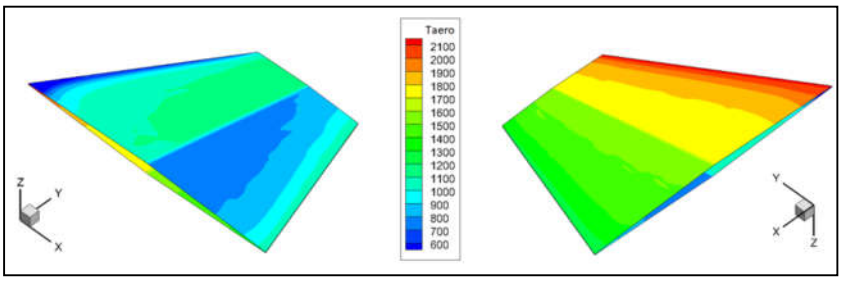

Figure 23 Temperature distribution of the upper surface (left) and lower surface (right) of the optimized wing surface at 100s

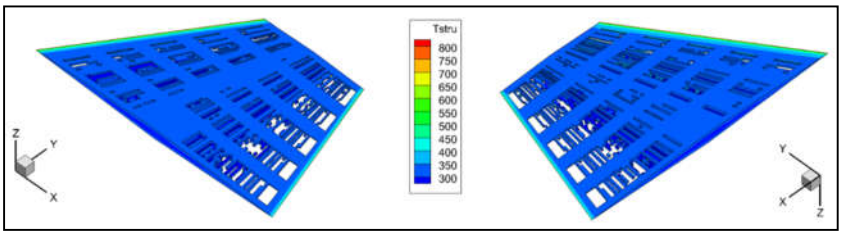

Figure 24 Temperature distribution of the upper surface (left) and lower surface (right) of the optimized wing structure layer at 100s

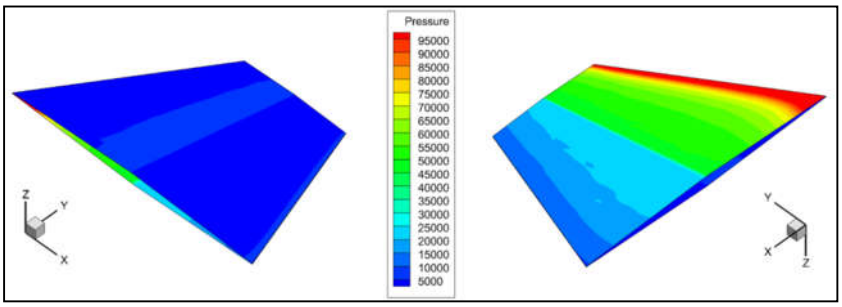

Figure 25 Pressure distribution of the upper surface (left) and lower surface (right) of the optimized wing surface at 100s

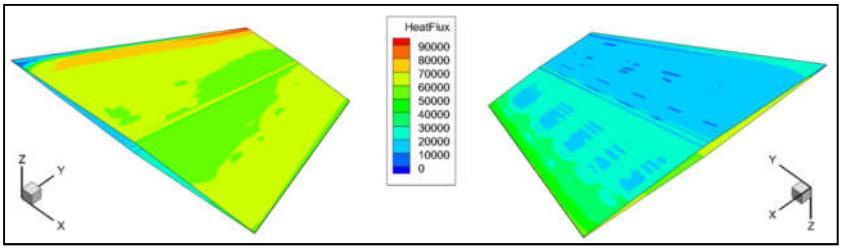

Figure 26 Heat flow distribution of the upper surface (left) and lower surface (right) of the optimized wing surface at 100s

4.3 Smooth processing of topology optimization results

As shown in Figure 20, the structure of the wing after density screening is not clear enough with many scattered structures. In order to be applied in engineering practice, the optimized result needs to be processed.

As can be seen from the optimized density distribution of hypersonic wing structure elements in Figure 21 and Figure 22, there are four obvious (element density is about 0.8) transverse structures (in the flow direction) on the wing surface and two obvious longitudinal structures (in the direction of wingspan) on the middle chord of the lower surface of the wing surface. The lower wing retains most of the elements. Referring to the wing structure with reinforced plates, the topology of the wing structure is shown in the figure below after processing the optimized area.

The maximum aerodynamic deformation, the maximum thermal deformation and the maximum total deformation of the processed hypersonic wing structure are obtained by the three-field coupling analysis. The results are compared with the original model and the optimized model as shown in Table 2.

By comparing the proceeded and optimized wing structure models, it can be seen that the overall deformation ratio increases slightly while the volume ratio increases from 60% to 67.3%.This is mainly because the smoothing process is manually revised by experience, and some of the additional reinforcing structures may be redundant, but it is acceptable from the perspective of engineering manufacturing.

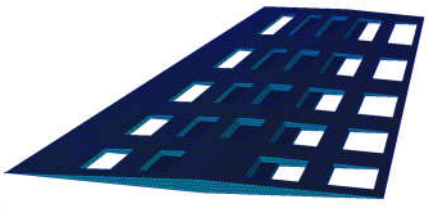

Figure 27 The processed optimized wing structure

Table 2 Comparison of wing structure deformation and volume ratio

Results at 100s	$u_{\max,F}$ /mm	$u_{\max,T}$ /mm	$u_{\max}$ /mm	The ratio of volume
The original model	15.5	102.6	112.5	100%
The optimization model	18.9	113.6	128.3	60.0%
The processed model	19.2	113.8	128.1	67.3%

4.4 Three-field coupling analysis and verification of the processed wing structure

The three-field coupling analysis with a flight duration of 600s is performed for the processed structure as calibration. Figure 28 to Figure 31 show the temperature, pressure and heat flow distribution of the processed structure. By comparing the results of the three-field coupling analysis for the original model, it can be seen that the temperature distribution and pressure distribution of the aerodynamic surface of the processed wing structure are similar to those of the original model. The temperature of the internal structure layer increases a little. The isothermal curve at about 600K shrinks slightly towards the center of the structure. The heat flow distribution results show that although the processed model and the original model are both in the heat flow equilibrium state, the heat flow in the hole area of the structure is negative, indicating that the heat dissipation capacity of the optimized structure is enhanced..

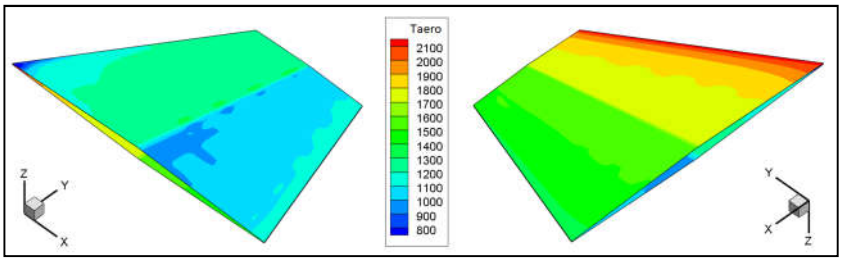

Figure 28 Temperature distribution of the upper surface (left) and lower surface (right) of the processed wing surface at 100s

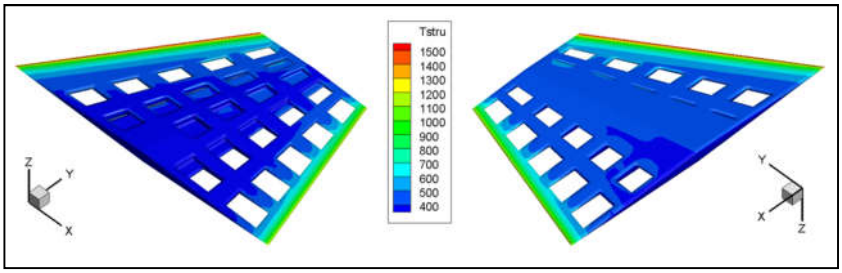

Figure 29 Temperature distribution of the upper surface (left) and lower surface (right) of the processed wing structure layer at 100s

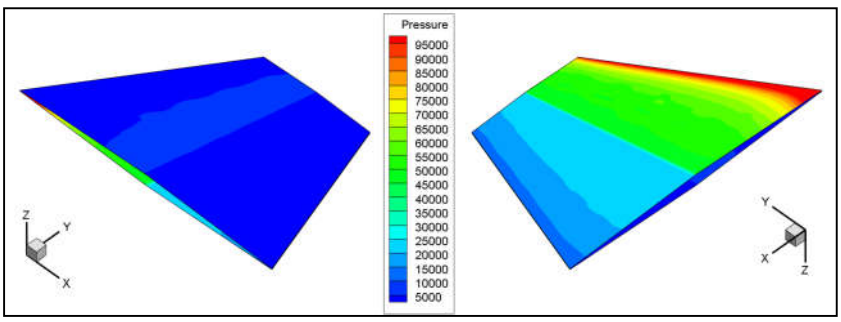

Figure 30 Pressure distribution of the upper surface (left) and lower surface (right) of the processed wing structure layer at 100s

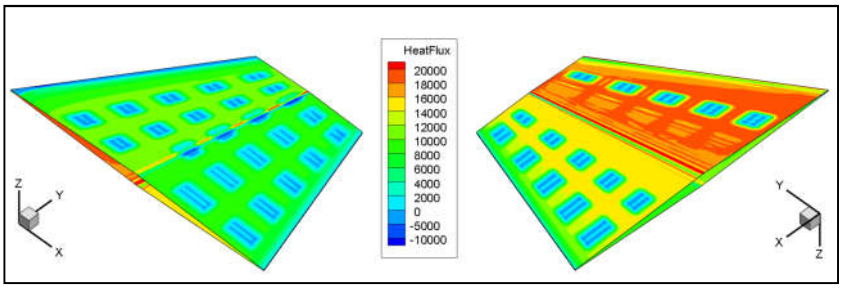

Figure 31 Heat flow distribution of the upper surface (left) and lower surface (right) of the processed wing structure layer at 100s

It can be seen from Table 2 that the deformation of the processed structure is more obvious than that of the original model. Therefore, the variation curves of the maximum aeroelastic deformation and the maximum thermal deformation with time and the distribution cloud map of the wing structure deformation at 600s are presented in Figure 32 to Figure 36.

The aeroelastic deformation of the processed structure increases significantly compared with the original model, while the temperature distribution of the internal structure layer of the wing surface changes slightly after optimization. Therefore, the increase of aeroelastic deformation at 600s is mainly affected by the reduction of stiffness after material reduction.

In addition, the aeroelastic deformations at 0s, extreme point, 200s and 600s of the processed structure are compared with those of the original model, as shown in Table 3.

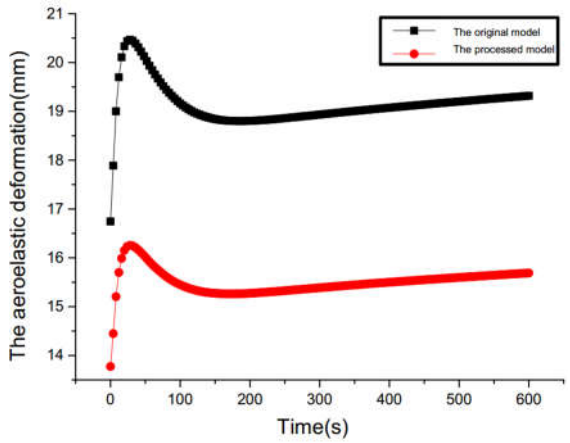

Figure 32 The displacement at the maximum aeroelastic deformation

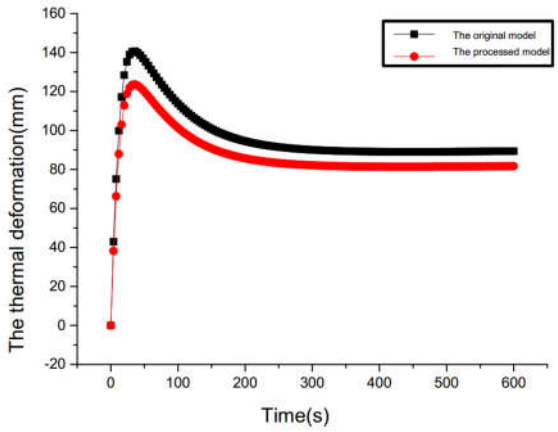

Figure 33 Thermal deformation curve at the maximal displacement

Table 3 Comparison of aeroelastic deformation of wing structure

The aeroelastic deformation	u_0 /mm	u_E /mm	Δu_E /mm	u_{200} /mm	Δu_{200} /mm	u_{600} /mm	Δu_{600} /mm
The original model	13.77	16.26	2.49	15.27	1.50	15.69	1.92
The processed model	16.74	20.46	3.72	18.80	2.06	19.32	2.58

The symbol Δ in Table 3 represents the deformation deviation between this moment and 0s. By comparing Δu_E of the processed structure and the original model, the reduced stiffness has a greater influence on the extreme value, and the processed structure is more susceptible to the impact of thermal load. In addition, according to Δu_{600}, the variation of the aeroelastic deformation

of the processed structure with a stable thermal environment relative to the initial value is also greater than that of the original model. However, by comparing Δu_{600} and Δu_{200}, it can be seen that the growth rate of aeroelastic deformation with time remains unchanged after the thermal environment is stable before and after optimization.

Table 4 Deformation comparison of airfoil structure

Deformation	u_E^A/mm	u_{600}^A/mm	u_E^T/mm	u_{600}^T/mm
The original model	16.26	15.69	123.63	81.68
The optimization model	20.46	19.32	140.62	89.40
The processed model	4.20	3.63	16.99	7.72

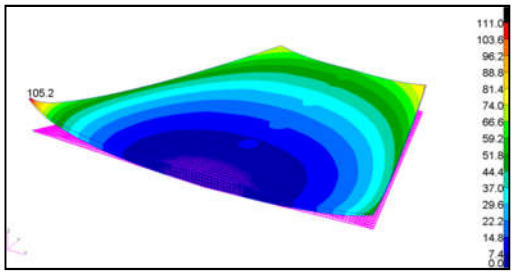

Figure 34 The overall deformation diagram of the processed wing structure at 600s

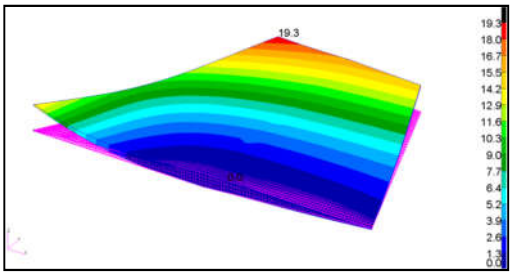

Figure 35 The aeroelastic deformation diagram of the processed wing structure at 600s

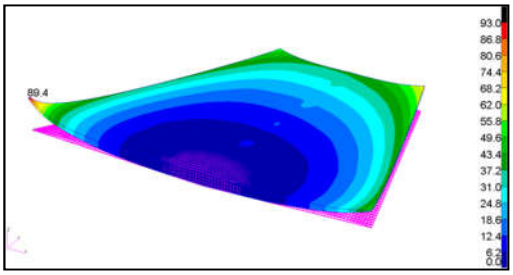

Figure 36 The thermal deformation diagram of the processed wing structure at 600s

The thermal deformation results in Figure 33 show that the reduction of structural layer material has little influence on the thermal deformation after the thermal environment is stable, but a big influence on the thermal deformation of the extreme point, and a similar influence on aeroelastic deformation as shown in Table 4 (Superscript A for aeroelastic deformation, T for thermal deformation, E for extreme value).

5. Conclusions

In this paper, a comprehensive optimization framework of wing structure for hypersonic vehicle is established, and the comprehensive optimization design of a typical wing structure of hypersonic vehicle with a small ratio and rhombic airfoil is carried out. The results of optimization process and structural deformation of the wing structure are compared and analyzed. After the topology optimization, the structure compliance is reduced, the mass decreases, and the volume ratio and displacement meet the specified constraints. As the optimization goes on, the proportion of thermal deformation in total deformation decreases gradually, and the heat loads transfer more favorably with the optimization. After smoothing the optimized results, a hypersonic wing topological structure is obtained with clear structure form close to engineering practice.

References

[1] Anderson J D . Hypersonic and High-Temperature Gas Dynamics[M], 2nd ed., AIAA, Reston, VA, 2006.

[2] Bertin J. J., Cummings R. M., Fifty Years of Hypersonics: Where We've Been and Where We're Going[J], Progress in Aerospace Sciences, 2003, 39(6-7): 511–536.

[3] Eli, Livne, Terrence et al., Aeroelasticity of Nonconventional Airplane Configurations: Past and Future[J], Journal of Aircraft, 2003, 40(6): 1047–1065.

[4] Zishka E., Agarwal R. K., Shape Optimization of a Blunt Body in Reacting Hypersonic Flow in Chemical Non-Equilibrium for Reducing Both Drag and Heat Transfer[J], AIAA Aviation, 22-26 June 2015, Dallas, TX.

[5] Preller D., Smart M., Design of an Minimum Trim Hypersonic Airbreathing Accelerator Vehicle[C], 18th AIAA/3AF, 24 - 28 September 2012, Tours, France.

[6] CHE Jing, Research on Optimal Design of Hypersonic Vehicle Waving Layout [D]. Doctoral Dissertation of Northwestern Polytechnical University, 2006. (In Chinese)

[7] Wang Yaokun, Research on Comprehensive Optimal Design Method of Hypersonic Vehicle with Thermoelasticity[D]. Doctoral Dissertation of Beihang University, 2015. (In Chinese)

[8] Kazmar R. R., Airbreathing Hypersonic Propulsion at Pratt and Whitney: Overview[R], AIAA 2005-3256, 2005.

[9] Bertin J. J., Hypersonic Aerothermodynamics[M], AIAA, Reston, VA,1994.

[10] Gaitonde D. V., Magnetohydrodynamic Energy Bypass Procedure in a Three-Dimensional Scramjet[J], Journal of Propulsion and Power, 1971, 22(3): 498–510.

[11] Bisplinghoff, R. L., Some Structural and Aeroelastic Considerations of High-Speed Flight[J], Journal of the Aeronautical Sciences, 1956, 23(4): 289–329, 367.

[12]Jack J. McNamara, and Peretz P. Friedmann, Aeroelastic and Aerothermoelastic Analysis in Hypersonic Flow: Past, Present, and Future[J], AIAA Journal, 2011, 49(6): 1089-1122

[13]Guoshu Li. Study on Aero-thermo-structure Coupling Analysis Method for Hypersonic Vehicle [D]. Ph.D. Thesis, Beihang University, 2013. (In Chinese)

[14]Qian Yiji, Aerodynamics [M]. Beijing: Beihang University Press, 2011. (In Chinese)

[15]Lighthill M. J., Oscillating Airfoils at High Mach Numbers[J], Journal of the Aeronautical Sciences, 1953, 20(6): 402–406.

[16]Eckert, E. R. G., Engineering Relations for Heat Transfer and Friction in High-Velocity Laminar and Turbulent Boundary-Layer Flow Over Surfaces With Constant Pressure and Temperature[J], Transactions of the ASME, 1956, 78(6): 1273–1283.

[17]Culler, A. J., and McNamara, J. J., Studies on Fluid–Thermal–Structural Coupling for Aerothermoelasticity in Hypersonic Flow[J], AIAA Journal, 2010, 48(8): 1721–1738.

[18]Culler A. J., McNamara J. J., Studies on Fluid–Thermal–Structural Coupling for Aerothermoelasticity in Hypersonic Flow[J], AIAA Journal, 2010, 48(8): 1721–1738

[19]Jinping Li. Analysis Method of Uncertainty Temperature Field and Structure[D]. Xi'an University of Electronic Science and Technology. 2008 (In Chinese)

[20]WANG Chengen, CUI Dongliang, QU Rongxia, et al. Finite Element Method and Application for Heat Transfer and Structure Analysis [M]. Beijing: Science Press, 2012. (In Chinese)

[21]Peter D. Dunning, Bret K. Stanford and H. Alicia Kim, "Level-Set Topology Optimization with Aeroelastic Constraints", AIAA SciTech, 5-9 January 2015, Kissimmee, Florida.

[22]Kazmar, R., Airbreathing Hypersonic Propulsion at Pratt and Whitney: Overview[R], AIAA 2005-3256, 2005.

[23]L. Yin, G. K. Ananthasuiesh. Topology Optimization of Compliant Mechanisms with Multiple Materials Using a Peak Function Material Interpolation Scheme[J]. Struct Multidisc Optim, 2001(23):49-62.

[24]Jiachun Li, Bangyan Ye, Yong Tang, et al. Algorithm for Topological Optimization of Thermal Conductive Structure Based on Density Method[J]. Journal of South China University of Technology(Natural Science Edition), 2006, 34(2):27-32. (In Chinese)